

This is the Submitted version (post-print) of the following paper: elastolytic-sensitive 3d-printed chitosan scaffold for wound healing applications by Catanzano et al. published on MRS Communications Volume 11, pages 924–930, (2021) DOI: <https://doi.org/10.1557/s43579-021-00124-x>. The final published version is available on the publisher website

1                   **ELASTOLYTIC-SENSITIVE 3D-PRINTED**  
2                   **CHITOSAN SCAFFOLD FOR WOUND HEALING**  
3                   **APPLICATIONS**  
4

5   Ovidio Catanzano, Department of Life Sciences, University of Trieste, Via Licio Giorgieri, 1,  
6   34127 Trieste, Italy; Institute for Polymers, Composites and Biomaterials  
7   (IPCB) – CNR, Via Campi Flegrei, 34, Pozzuoli, Naples, Italy  
8

9   Lisa Elviri, Carlo Bergonzi, Annalisa Bianchera, and Ruggero Bettini, Food and Drug  
10   Department, University of Parma, Parco Area delle Scienze 27/A, 43124 Parma, Italy  
11

12   Antonella Bandiera, Department of Life Sciences, University of Trieste, Via Licio Giorgieri,  
13   1, 34127 Trieste, Italy  
14

15  
16   Address all correspondence to Ovidio Catanzano at [Ovidio.catanzano@ipcb.cnr.it](mailto:Ovidio.catanzano@ipcb.cnr.it)  
17

18   **Abstract**

19   The combination of a chitosan 3D-printed scaffold with a hydrogel matrix containing an  
20   elastin-like polypeptide functionalized with the epidermal growth factor (HEGF) was  
21   evaluated as a possible strategy to obtain a bioactive platform with stimuli-responsive  
22   properties. We designed a chitosan/ HEGF hybrid scaffold and examined the physico-  
23   chemical properties and the in vitro behavior when in contact with simulated biological fluids.  
24   Primary human dermal fibroblasts (hDFs) were used to test the in vitro cytocompatibility.  
25   Overall, these data provide first insights into the integration of HEGF-based hydrogel with  
26   3D-printed scaffolds, contributing towards the rational design of a new smart functional  
27   wound dressing.  
28

## 29 **1. Introduction**

30 Recently, bio-inspired polypeptides such as the elastin-like polypeptides (ELPs) have  
31 proved to be excellent as components for drug delivery and tissue engineering applications  
32 due to their good cytocompatibility and biocompatibility, their ease of handling and design,  
33 production, and modification.[1-3] The interest towards these recombinant biopolymers is  
34 based on the fundamental role of the native elastin protein in the extracellular matrix that  
35 confers rubber-like elasticity to the tissues, allowing them to be subjected to indefinite cycles  
36 of deformation/relaxation without rupture. Most of the elastin-like polypeptides currently  
37 used for tissue engineering applications are derived from the recombinant expression of the  
38 repeated bovine aminoacidic motifs, and the human recombinant version of these elastin-  
39 like sequences has been developed as an alternative to be used in tissue engineering.  
40 Human Elastin-Like Polypeptides (HELPS) are artificial, recombinant biopolymers based on  
41 the hexapeptidic VAPGVG repeated motif of human elastin.[1] Interestingly, thanks to the  
42 presence of glutamine and lysine residues in their primary structure, HELPS can be cross-  
43 linked under the action of transglutaminase (TG) to form stable hydrogels without the use of  
44 harsh chemicals like glutaraldehyde or analogous cross-linking agents.[4] HELP-based  
45 biomaterials have already shown high potential to be employed for many applications in  
46 tissue engineering, regenerative medicine, and cell encapsulation,[5] as well as to prepare  
47 biomimetic surfaces for cell culture,[6] and for the delivery of biological therapeutic  
48 agents.[7,8] Moreover, the use of recombinant HELP opens the possibility to incorporate  
49 bioactive sequences that contribute to the development of new bioactive materials that can  
50 be applied in tissue regeneration.[9] The features of ELPs make them also useful for the  
51 design of swellable, adaptable, and elastic wound dressings, finely tailoring their structural  
52 and mechanical properties. However, despite all these promising characteristics, very little  
53 work has been performed on ELPs in the field of wound healing.[2] One of the main  
54 drawbacks lies in the poor rheological characteristics of the derived hydrogel matrix that  
55 results inadequate for applications on difficult-to-heal wounds. The management of chronic  
56 wounds is currently based on the use of robust wound dressings as they provide better  
57 exudate management and prolonged residence at the wound site.[10] To overcome this  
58 problem, the integration of the HELP-based hydrogel with 3D-printed polymeric scaffolds  
59 may represent a successful strategy to preserve the bioactive properties of the HELP  
60 hydrogel as well as to increase the mechanical and handling performance of the scaffold.  
61 The application of 3D printing in the wound healing field is particularly interesting, especially  
62 when combined with 3D scanning, to create personalized dressings, adapted in shape and

63 size to individual patients.[11] Recently, an innovative extrusion-based 3D printing technique  
64 combined with freeze-gelation has been proposed to prepare chitosan scaffolds to be  
65 applied in the regenerative skin tissue field.[12] Chitosan is a very versatile semi-synthetic  
66 polymer derived from the alkaline N-deacetylation of chitin, the main structural component  
67 of the crustacean exoskeleton, and finds most of its application in wound dressings, scaffold,  
68 and as antimicrobial agent.[13] It is a biodegradable and biocompatible polymer that  
69 possesses antibacterial, hemostatic, and bioadhesive characteristics,[14] all desirable  
70 features for ideal wound dressings. In addition, the easy chemical modification and favorable  
71 rheological characteristics have prompted the use of chitosan and its composites as bio-  
72 inks for 3D-printed biomaterials.[15,16] For this reason, chitosan-based wound dressings  
73 are extensively studied to favor wound closure, prevent wound infections, and control the  
74 release of drugs and growth factors at wound sites to stimulate and improve wound healing.  
75 The use of recombinant techniques to produce HELPs offers several advantages as well.  
76 Modified versions of HELP functionalized with bioactive molecules can be easily prepared,  
77 as in the case of the fusion of HELP with the epidermal growth factor (EGF) that has been  
78 recently synthesized in our laboratory. [17] EGF, together with its receptor (EGFR) plays an  
79 essential role in wound healing by stimulating epidermal and dermal regeneration [18,19]  
80 but its use in wound care has been limited so far by its short half-life, resulting from the rapid  
81 in vivo degradation, and by the limited efficacy of the delivery methods. By introducing EGF  
82 sequence within the backbone of HELP, we obtained a fusion protein (HEGF) maintaining  
83 both the EGF bioactivity and the responsivity to a proteolytic environment, such as a wound  
84 site.[20] The study reported here focuses on the development of a new composite scaffold  
85 that combines the flexibility of the 3D printing technique with the stimuli-induced release  
86 ability of a HEGF hydrogel. High-porosity chitosan 3D-printed scaffolds (CHIT) were  
87 embedded by enzymatic cross-linking in HEGF-enriched HELP matrix and the interaction  
88 between these components as well as the release of EGF from the scaffold was evaluated.  
89 Finally, primary human Dermal Fibroblasts (hDFs) were used to test the in vitro  
90 cytocompatibility of the scaffolds.

91

## 92 **2. Materials and methods**

### 93 **2.1. Material development and scaffold fabrication via extrusion-based** 94 **3D printing**

95 HELP recombinant biopolymer and its modified fusion with the EGF (HEGF) were prepared  
96 as previously reported.<sup>[7]</sup> The recombinant products were expressed in a C3037 E. coli strain  
97 (New England Biolabs, Ipswich, MA) and then subjected to an extraction and purification  
98 procedure. The separation of the recombinant biopolymers of interest from the supernatant  
99 was obtained exploiting the inverse phase transition properties using a series of  
100 temperature-dependent transition cycles. Three of these cycles were sufficient to obtain the  
101 pure recombinant protein. The polypeptide was frozen overnight at  $-80^{\circ}\text{C}$ , and then  
102 lyophilized at 0.01 atm and  $-60^{\circ}\text{C}$  in a Modulyo apparatus (Edwards, Crawley, UK) for long-  
103 term storage. The yield and the purity of the recombinant polypeptides obtained were  
104 evaluated by sodium dodecyl sulfate-polyacrylamide gel electrophoresis (SDS-PAGE).  
105 Chitosan Chitoclear™ (CAS 9012-76-4, degree of deacetylation 95%; molecular weight  
106 150–200 kDa) from PRIMEX Ehf (Siglufjordur, Iceland) was used for 3D printing. The  
107 preparation and characterization of the 3D-printed scaffolds employed in this study were  
108 already described by Elviri et al. [21] The 3D printing system was conceived as an  
109 automation of a freeze-gelation method for the preparation of chitosan scaffolds with  
110 controlled porosity, to have a precise and accurate control of the scaffold geometry. Briefly,  
111 a chitosan solution (4% w/v) in 1% v/v aqueous acetic acid solution was loaded in a 5 mL  
112 syringe mounting a 26 G needle (inner diameter 192  $\mu\text{m}$ ). The syringe was fixed in an in-  
113 house built 3D printer and the solution was extruded on a cooled surface and instantly frozen  
114 to fix the grid structure composed by overlapping orthogonal filaments with an inter-filament  
115 distance of 200  $\mu\text{m}$ . For the performed experiments, 5-layer scaffolds were produced. At the  
116 end of each printing process, the frozen hydrogel underwent ionotropic gelation that  
117 occurred in potassium hydroxide 1.5 M (pH 14). After 1 h of immersion, scaffolds were  
118 washed in ultrapure water till neutrality.

119

## 120 **2.2. Composite chitosan/HEGF wound dressings preparation**

121 To prepare the CHIT/HEGF composites, HELP and HEGF were enzymatically cross-linked  
122 resulting in a matrix embedding the CHIT scaffolds. Before the cross-linking, the scaffolds  
123 were cut in a 5-mm-diameter disk using a stainless-steel punch, frozen overnight at  $-80^{\circ}\text{C}$ ,  
124 and lyophilized at 0.01 atm and  $-60^{\circ}\text{C}$  in a Modulyo apparatus (Edwards, UK). To prepare  
125 the matrix, a 4% (w/v) solution of HEGF and HELP was prepared dissolving the lyophilized  
126 proteins in cold 10 mM Tris/HCl (Sigma-Aldrich, USA), pH 8. HEGF-loaded composites were  
127 fabricated employing 20  $\mu\text{L}$  of a precooled 4wt% HEGF/HELP (1:19) solution that was mixed  
128 with 2  $\mu\text{L}$  of microbial transglutaminase (60 mg/mL) and quickly dropped onto the surface of

129 the CHIT 3D-printed scaffold in a vertically placed cylindrical mold. The mold was then  
130 centrifuged at 1500 rpm for 3 min to achieve a homogenous gel distribution in the porous  
131 scaffold. The cross-linking was completed after 2-h incubation at room temperature. After  
132 the reaction, the composite dressings were gently removed from the mold, washed  
133 extensively with ultrapure water at 4°C overnight, frozen overnight at – 80°C, and finally  
134 lyophilized at 0.01 atm and – 60°C in a Modulyo apparatus (Edwards, UK). The CHIT/HEGF  
135 composites scaffolds were stored in desiccators over silica gel at room temperature until  
136 use.

137

### 138 **2.3. Physico-chemical characterization of the printed CHIT/HEGF** 139 **composites**

140 The surface morphology of CHIT/HEGF composites was analyzed through a stereoscopic  
141 microscope (Olympus SZ61TR) and scanning electron microscopy (SEM) (Philips Model  
142 501). To collect the SEM images, the samples were mounted on a metal stub by means of  
143 carbon adhesive tape and coated with a 20-nm-thick gold/palladium. The average porosity  
144 and the density of CHIT/HEGF composite wound dressings were determined by a fluid  
145 displacement method, using ethanol as the displacement liquid.[22] The pore average  
146 diameters were calculated measuring at least 100 pores from three different SEM images  
147 using the public domain ImageJ software 1.52v (NIH, Bethesda, MD, USA). Water uptake  
148 was determined by placing the CHIT and CHIT/HEGF composite wound dressing in water.  
149 The initial weight of each sample was accurately recorded using an analytical balance, and  
150 then they were placed in 20 mL of water in a thermostatic bath at 37°C. Samples were taken  
151 out, excess water was carefully removed using tissue paper, and after being weighed were  
152 re-immersed in water. The sample weight was recorded after 15 and 30 min, 1, 2, 4, 6 h and  
153 from there onwards until equilibrium was established after 24 h. The percentage swelling  
154 ratio (SR%) at each time point was calculated using Eq. (1):

155

$$156 \quad \text{SR}\% = \frac{W - W_0}{W_0} \times 100, \quad (1)$$

157

158

159 where  $W$  is the mass of the swollen sample and  $W_0$  is the mass of the initial dry sample. The  
160 equilibrium water content (EWC) percent was calculated by Eq. (2):

160

$$\text{EWC}(\%) = \frac{W_e - W_d}{W_e} \times 100, \quad (2)$$

161

162 where  $W_e$  is the mass of the swollen sample at equilibrium and  $W_d$  is the mass of the dry  
163 sample at equilibrium. The interaction of CHIT and CHIT/HEGF composite with the proteins  
164 was evaluated using the solution depletion technique. Both the 3D-printed CHIT scaffold  
165 and the CHIT/HEGF composite were immersed in 5 mL of Bovine Serum Albumin (BSA)  
166 solution 1 mg/mL (Sigma-Aldrich, USA) in PBS pH 7.4. After 24 h of incubation at 37°C, the  
167 amount of adsorbed protein was calculated from the differences in the BSA concentration  
168 before and after immersion of the composites. The Bradford reagent was used for the  
169 quantification of the protein absorbed by hydrogels. Briefly, 5  $\mu$ L of the samples were mixed  
170 with 250  $\mu$ L of the Bradford reagent and incubated in the dark at room temperature for 1 h  
171 before analysis. The absorbance (ABS) of the samples was measured at 595 nm using a  
172 Synergy H1 Hybrid Multi-Mode Reader (BioTek Instruments, Inc., USA). Results were  
173 expressed as the difference between the ABS of the control 1 mg/mL BSA solution and the  
174 ABS of the same solution that came into contact with the samples. The in vitro stability of  
175 the CHIT/HEGF composite was tested immersing the constructs in simulated wound fluid  
176 (SWF) composed as follows: 0.4 M NaCl, 2 mM CaCl<sub>2</sub>, 8 mM TRIS, all obtained from Sigma-  
177 Aldrich (USA). To simulate a proteolytic environment, elastase (0.5  $\mu$ g/mL) was added to  
178 the SWF. The weight loss during immersion in SWF was measured by recording the weight  
179 changes of the dry specimen after the specified incubation time. Briefly, different sets of  
180 samples ( $n = 4$ ) were immersed in 5 mL of SWF containing 2.5  $\mu$ g of elastase at 37°C for 48 h.  
181 Material dissolution was evaluated in terms of weight loss in relation to the immersion time.  
182 After 6, 24, and 48 h, the composites were removed from the fluid, rinsed with ultrapure water,  
183 and finally, lyophilized at 0.01 atm and - 60°C in a Modulyo apparatus (Edwards, UK) after overnight  
184 freezing at - 80°C. The percentage of weight loss (WL) was calculated according to Eq. (3):

185

$$\text{WL}\% = \frac{W - W_0}{W_0} \times 100, \quad (3)$$

186

187

188 where  $W$  is the mass of the sample at time  $t$  and  $W_0$  is the mass of the initial dry sample.  
189 Degradation studies were conducted with CHIT/HEGF composite and with the unloaded  
190 CHIT scaffolds.

191

## 192 **2.4. Evaluation of EGF release from the CHIT/ HEGF composite wound** 193 **dressing**

194 The CHIT/HEGF composite wound dressings were washed with excess water to ensure the  
195 removal of any unbound or unreacted component. The lyophilized dressings described  
196 above were first soaked in 500  $\mu$ L of digestion buffer (50 mM Tris/HCl pH 7.5, 1 mM CaCl<sub>2</sub>)  
197 at 37°C for 16 h, the supernatant (named T<sub>0/n</sub>) was sampled and stored at – 20°C before  
198 analysis. Then, the CHIT/HEGF dressings were immersed in 700  $\mu$ L of the 50 mM Tris/HCl  
199 pH 7.5, 1 mM CaCl<sub>2</sub> buffer added of elastase from porcine pancreas (Sigma-Aldrich, USA,  
200  $\geq 4$  units/ mg) to a final concentration of 0.5  $\mu$ g/mL. 200  $\mu$ L of this supernatant was  
201 immediately removed (T<sub>0</sub>) and stored at – 20°C for subsequent analysis. The composite  
202 was further incubated at 37°C in the remaining 500  $\mu$ L with the elastase enzyme. After 2 h,  
203 50  $\mu$ L of supernatant was collected and stored at – 20°C for subsequent analysis. For  
204 volume replacement, 50  $\mu$ L of the fresh buffer with elastase were added to the sample to  
205 continue the incubation at 37°C. The same procedure was repeated after 4 and 8 h. The  
206 supernatants deriving from the EGF release assays were analyzed for EGF content by a dot  
207 blot procedure as described in the supplementary material.

208

## 209 **2.5. Cell culture and cytotoxicity assay**

210 Biological investigations on HEGF-loaded composite wound dressing were performed using  
211 human dermal fibroblasts (hDFs). Primary human fibroblasts were isolated, with informed  
212 consent, from a healthy, normolipemic 45-year-old female. hDFs, coded as C84, were grown  
213 in Minimum Essential Eagle Medium (MEM) (Thermo Fisher Scientific, USA) with 10% Fetal  
214 Bovine Serum (FBS), antibiotic solution (streptomycin 100 IU/mL and penicillin 100 IU/mL),  
215 and 2 mM L-glutamine (all obtained from Aurogene, Italy), at 37°C in a wet atmosphere with  
216 5% CO<sub>2</sub>. The cytotoxicity assay was performed by first culturing hDFs on CHIT/HEGF  
217 dressings and then evaluating the viability of the cells using the resazurin assay. The  
218 detailed procedure is reported in the supplementary material.

219

## 220 **3. Results**

221 An interesting strategy for enhancing the structural integrity and fracture toughness of  
222 hydrogels is forming a composite by incorporating a 3D-printed scaffold as a structural  
223 element.[23,24] Following the deposition scheme provided by the 3D printer (Fig. 1(a)),  
224 CHIT scaffolds show a regular grid structure (Fig. 1(b)) and can be handled without the risk



225 of breaking. On the other hand, cross-linked HELP-based matrices were proved to be  
226 structurally too weak, and for this reason, we decided to strengthen this hydrogel preparing  
227 a composite material by using a mixture of HELP and HEGF and performing the enzymatic  
228 cross-linking directly on the 3D CHIT scaffolds.[4] The cross-linking takes place through the  
229 formation of isopeptide bonds among lysine and glutamine residues available on the HELP  
230 domain, present in HEGF as well, mimicking a process that occurs in nature avoiding the  
231 use of chemical or physical harsh conditions. After washing and freeze-drying, CHIT and  
232 CHIT/HEGF dressings have a regular and elegant shape, with adequate handling properties  
233 to withstand the requirement for a wound application (Fig. 1(c) and (d), respectively). The  
234 preparation method developed here is simple and leads to the formation of a complex  
235 porous architecture characterized by two well-separated microstructures. In Fig. 2,  
236 representative SEM images of the surface of the CHIT/HEGF composites are shown. In  
237 these images, the complex microstructure is well highlighted, with the porous  
238 interconnecting network of polymeric strands having irregularly shaped pores with thin walls.  
239 It has already been reported that the activity of transglutaminase on HELP solutions resulted  
240 in hydrogel matrices with a porous structure.[4] In the magnification of Fig. 2, the pore size  
241 difference of the two materials is clearly visible, with an open cell structure with an average  
242 diameter of  $86.5 \pm 23.3 \mu\text{m}$  formed by the HEGF-loaded HELP matrix and a smaller chitosan  
243 interconnected network characterized by pores with an elongated shape and an average  
244 diameter of  $30.3 \pm 10.9 \mu\text{m}$ . This peculiar morphology of CHIT/ HEGF composite has a  
245 significant impact on the ability of the dressing to absorb water, increasing the swelling ratio  
246 after 24 h from  $494.4\% \pm 72.2\%$  to  $1125.0\% \pm 52.9\%$  (Table I). For a dressing, the ability to  
247 absorb fluids and retain moisture without leaking is essential for the final application, as the  
248 accumulation of excess exudate on the wound site slows down the healing process and  
249 causes skin maceration.[10] At the same time, the rate and duration of swelling determine  
250 the ability of the dressing to control drug release over a prolonged period, a process  
251 generally driven by fluid uptake and diffusion. When looking at swelling profiles of scaffolds  
252 with respect to time (Fig. 3(a)), besides the higher swelling capacity by CHIT/ HEGF  
253 composite compared to CHIT scaffold, it is interesting to notice that the swelling rate is  
254 significantly different. CHIT dressing reaches its maximum within 30 min, while CHIT/ HEGF  
255 reaches it in an hour at least. The comparison of CHIT and CHIT/HEGF with the HELP plain  
256 matrix was not possible due to the very poor handling properties of the HELP after hydration,  
257 confirming the need for chitosan 3D-printed scaffolds as an essential structural component  
258 of the proposed system.

259 Among the parameters that can affect the kinetics of water uptake, the different pore size of  
260 the material is one of the most prominent. The EWC represents the amounts of fluids that a  
261 material can absorb in relation to its weight. As for the swelling profiles, the results reveal  
262 that the EWC is significantly higher for the CHIT/HEGF dressing (Table I). An EWC value  
263 similar to the fluid contents of living tissues (about 60%) is considered a good indicator of  
264 the compatibility of these materials with the wound area. Finally, the low porosity and density  
265 of CHIT/ HEGF, calculated with the fluid replacement method, suggest a relatively compact  
266 material, but which still maintains the ability to absorb fluids, due to the significant differences  
267 in water absorption and EWC. When a dressing comes into contact with wound exudate,  
268 the exudate proteins almost immediately start to adsorb to the surface, eliciting foreign body  
269 reactions, triggering the inflammatory response, and delaying the wound healing process.  
270 This phenomenon is strongly related to the adsorption of water molecules but is also  
271 dependent on the surface composition of the (bio)material that comes in contact with the  
272 wound environment. [25] Because of its high concentration in wound exudate and moderate  
273 size, albumin dominates initial interactions with the surface and for this reason, we simulated  
274 the adsorption of exudate proteins onto CHIT and CHIT/HEGF composites using a Bovine  
275 Serum Albumin (BSA) solution at pH 7.4 and 37°C. However, in this case, both the samples  
276 tested resulted to have a negligible interaction with the BSA, independently from the swelling  
277 properties of the materials (Fig. S1), which is usually the main driving force for protein  
278 adsorption at most interfaces. A feature of HELP-based hydrogels is their susceptibility to  
279 the action of neutrophil elastase, which causes the release of bioactive moieties.[26] The  
280 activity levels of neutrophil elastase were found significantly elevated in chronic wounds  
281 such as pressure ulcers and leg ulcers,[27,28] with no association with the condition of the  
282 wound.[29] CHIT/HEGF composites were investigated for their stability in SWF containing  
283 elastase to simulate the proteolytic environment generally present in a chronic wound (Fig.  
284 3(b)). Throughout the experiment, the activity of elastase on the degradation rates of 3D-  
285 printed CHIT structure is negligible and the slight chitosan weight loss could be explained  
286 by solubilization of non-cross-linked chitosan chains. In contrast, at each time point, there is  
287 a significant difference in weight loss on CHIT/HEGF dressings due to a selective HEGF-  
288 loaded HELP matrix degradation by elastase that does not affect the chitosan scaffold (Fig.  
289 3(b), Fig. S2). Our results showed a progressive HELP-based hydrogel matrix loss, which  
290 achieved complete degradation after 24 h, despite an inhibitory effect of chitosan on  
291 elastase activity has been reported.[30] Interestingly, this susceptibility to proteolysis of the  
292 HEGF-loaded HELP matrix can be exploited to trigger the release of active compounds

293 loaded in the matrix itself.[7] In our case, the CHIT/HEGF dressings were tested to verify  
294 the ability of an elastolytic stimuli-induced release of the EGF. The samples were first  
295 soaked in the release buffer alone, without any enzyme that can trigger the release. The dot  
296 blot analysis of the supernatants derived from the 16-h incubation of the composites in the  
297 absence of the elastase (To/n) did not show any chemiluminescent signal (data not shown)  
298 confirming that the enzymatic action of elastase is essential to trigger the EGF release from  
299 the dressings. On the contrary, after enzyme addition, chemiluminescent signals became  
300 detectable after about 8 h of incubation, which is also the time in which a large part of the  
301 HEGF matrix is degraded by the action of elastase (Fig. 3(c)). Taken together, the in vitro  
302 stability and the EGF release experiments confirmed that the proteolytic degradation of the  
303 HEGF-loaded matrix leads to the EGF local release from the composite. Results suggest  
304 that if applied in vivo, this composite may be activated by the elastolytic activity of the wound  
305 exudate, representing an attractive smart dressing with stimuli-responsive properties.  
306 Further studies are underway on the activity of the CHIT/HEGF composites applied to in  
307 vivo wound models for the evaluation of EGF release and its effects on wound  
308 progression.[20]

309 Preliminary biological investigations were performed to evaluate the occurrence of any  
310 cytotoxic effects and the ability of CHIT/HEGF dressing to support fibroblast viability, with  
311 respect to CHIT scaffold, whose cytocompatibility had been previously demonstrated.<sup>[12]</sup> The  
312 in vitro cytotoxicity evaluation is a fast method to provide predictive evidence of material  
313 biocompatibility. For wound healing applications, good cytocompatibility is desirable, as well  
314 as adequate physical properties and biodegradability. As shown in Fig. 3(d), CHIT/HEGF  
315 not only did not show any cytotoxic effect on hDFs, but also significantly improved their  
316 proliferation with respect to CHIT dressing. This suggests that in the hDF cultures the  
317 release of EGF in the growth medium may be induced, promoting cell proliferation.

318

## 319 **4. Conclusion**

320 Overall, here we describe a method to prepare a composite material by reinforcing the  
321 HEGF hydrogel with a 3D-printed chitosan scaffold, to ensure adequate mechanical strength  
322 to withstand the requirement for its application as a wound dressing. The peculiar  
323 morphology of CHIT/HEGF composite observed using SEM microscopy has a significant  
324 impact on the ability of the dressing to absorb body fluids. The susceptibility to enzymatic  
325 degradation of the HEGF-loaded matrix makes this composite sensitive to the proteolytic  
326 environments, an attractive feature to realize smart dressings with stimuli-responsive

327 properties. Further investigation will follow to better clarify the effect of the proteolytic  
328 environment on the EGF release mechanism and the in vivo activity of dressings based on  
329 these composites in a rabbit splinted-wound model.

330

331

## 332 **Acknowledgement**

333 This work was funded by “Commissariato del Governo della Regione Friuli Venezia Giulia -  
334 Fondo Trieste” and managed by AREA Science Park in the frame of “Made in Trieste”  
335 program. The authors wish to thank Dr. M. Stebel for technical assistance in HELP and  
336 HEGF polypeptide production and Prof. S. Passamonti for scientific assistance during the  
337 project.

338

## 339 **Data availability**

340 The datasets generated during and/or analyzed during the current study are available from  
341 the corresponding author on reasonable request.

342

## 343 **Conflict of interest**

344 On behalf of all authors, the corresponding author states that there is no conflict of interest.

345

## 346 **Supplementary Information**

347 The online version contains supplementary material available at [https:// doi. org/ 10. 1557/  
348 s43579- 021- 00124-x](https://doi.org/10.1557/s43579-021-00124-x).

349

350

351 **References**

- 352 1. G. Ciofani, G.G. Genchi, V. Mattoli, B. Mazzolai, A. Bandiera, The potential of  
353 recombinant human elastin-like polypeptides for drug delivery. *Expert Opin. Drug Deliv.* 11,  
354 1507 (2014)
- 355 2. J.C. Rodriguez-Cabello, I. Gonzalez de Torre, A. Ibanez-Fonseca, M. Alonso, Bioactive  
356 scaffolds based on elastin-like materials for wound healing. *Adv. Drug Deliv. Rev.* 129, 118  
357 (2018)
- 358 3. D.H.T. Le, A. Sugawara-Narutaki, Elastin-like polypeptides as building motifs toward  
359 designing functional nanobiomaterials. *Mol. Syst. Des. Eng.* 4, 545 (2019)
- 360 4. A. Bandiera, Transglutaminase-catalyzed preparation of human elastinlike polypeptide-  
361 based three-dimensional matrices for cell encapsulation. *Enzyme Microb. Technol.* 49, 347  
362 (2011)
- 363 5. A. Bandiera, Elastin-like polypeptides: the power of design for smart cell encapsulation.  
364 *Expert Opin. Drug Deliv.* 14, 37 (2017)
- 365 6. P. D'Andrea, D. Civita, M. Cok, L.U. Severino, F. Vita, D. Scaini, L. Casalis, P. Lorenzon,  
366 I. Donati, A. Bandiera, Myoblast adhesion, proliferation and differentiation on human elastin-  
367 like polypeptide (HELP) hydrogels. *J. Appl. Biomater. Funct.* 15, 43–53 (2017)
- 368 7. A. Bandiera, A. Markulin, L. Corich, F. Vita, V. Borelli, Stimuli-induced release of  
369 compounds from elastin biomimetic matrix. *Biomacromolecules* 15, 416 (2014)
- 370 8. G. Ciofani, G.G. Genchi, P. Guardia, B. Mazzolai, V. Mattoli, A. Bandiera, Recombinant  
371 human elastin-like magnetic microparticles for drug delivery and targeting. *Macromol.*  
372 *Biosci.* 14, 632 (2014)
- 373 9. S.M. Staubli, G. Cerino, I. Gonzalez De Torre, M. Alonso, D. Oertli, F. Eckstein, K. Glatz,  
374 J.C. Rodriguez Cabello, A. Marsano, Control of angiogenesis and host response by  
375 modulating the cell adhesion properties of an Elastin- Like Recombinamer-based hydrogel.  
376 *Biomaterials* 135, 30 (2017)
- 377 10. J. Boateng, O. Catanzano, Advanced therapeutic dressings for effective wound  
378 healing—a review. *J. Pharm. Sci.* 104, 3653 (2015)
- 379 11. A. Goyanes, U. Det-Amornrat, J. Wang, A.W. Basit, S. Gaisford, 3D scanning and 3D  
380 printing as innovative technologies for fabricating personalized topical drug delivery  
381 systems. *J. Control. Release* 234, 41 (2016)

- 382 12. C. Intini, L. Elviri, J. Cabral, S. Mros, C. Bergonzi, A. Bianchera, L. Flammini, P. Govoni,  
383 E. Barocelli, R. Bettini, M. McConnell, 3D-printed chitosan- based scaffolds: an in vitro study  
384 of human skin cell growth and an in-vivo wound healing evaluation in experimental diabetes  
385 in rats. *Carbohydr. Polym.* 199, 593 (2018)
- 386 13. R. Singh, K. Shitiz, A. Singh, Chitin and chitosan: biopolymers for wound management.  
387 *Int. Wound J.* 14, 1276 (2017)
- 388 14. I. Bano, M. Arshad, T. Yasin, M.A. Ghauri, M. Younus, Chitosan: a potential biopolymer  
389 for wound management. *Int. J. Biol. Macromol.* 102, 380 (2017)
- 390 15. S.S. Murugan, S. Anil, P. Sivakumar, M.S. Shim, J. Venkatesan, 3D-printed chitosan  
391 composites for biomedical applications, in *Chitosan for biomaterials IV: biomedical*  
392 *applications.* ed. by R. Jayakumar, M. Prabakaran (Springer International Publishing, Cham,  
393 2021), p. 87
- 394 16. J.R.H. Sta. Agueda, Q. Chen, R.D. Maalihan, J. Ren, Í.G.M. da Silva, N.P. Dugos, E.B.  
395 Caldona, R.C. Advincula, 3D printing of biomedically relevant polymer materials and  
396 biocompatibility. *MRS Commun.* 11, 197 (2021)
- 397 17. P. D'Andrea, M. Sciancalepore, K. Veltruska, P. Lorenzon, A. Bandiera, Epidermal  
398 Growth Factor-based adhesion substrates elicit myoblast scattering, proliferation,  
399 differentiation and promote satellite cell myogenic activation. *Biochim. Biophys. Acta Mol.*  
400 *Cell. Res.* 1866, 504 (2019)
- 401 18. S. Barrientos, H. Brem, O. Stojadinovic, M. Tomic-Canic, Clinical application of growth  
402 factors and cytokines in wound healing. *Wound Repair Regen.* 22, 569 (2014)
- 403 19. R.J. Bodnar, Epidermal growth factor and epidermal growth factor receptor: the Yin and  
404 Yang in the treatment of cutaneous wounds and cancer. *Adv. Wound Care (New Rochelle)*  
405 2, 24 (2013)
- 406 20. O. Catanzano, F. Quaglia, J.S. Boateng, Wound dressings as growth factor delivery  
407 platforms for chronic wound healing. *Expert Opin. Drug Deliv.* 1, 737–759 (2021)
- 408 21. L. Elviri, R. Foresti, C. Bergonzi, F. Zimetti, C. Marchi, A. Bianchera, F. Bernini, M.  
409 Silvestri, R. Bettini, Highly defined 3D printed chitosan scaffolds featuring improved cell  
410 growth. *Biomed. Mater.* 12, 045009 (2017)

- 411 22. O. Catanzano, V. D'Esposito, P. Formisano, J.S. Boateng, F. Quaglia, Composite  
412 alginate-hyaluronan sponges for the delivery of tranexamic acid in postextractive alveolar  
413 wounds. *J. Pharm. Sci.* 107, 654 (2018)
- 414 23. J. Visser, F.P. Melchels, J.E. Jeon, E.M. van Bussel, L.S. Kimpton, H.M. Byrne, W.J.  
415 Dhert, P.D. Dalton, D.W. Hutmacher, J. Malda, Reinforcement of hydrogels using three-  
416 dimensionally printed microfibrils. *Nat. Commun.* 6, 6933 (2015)
- 417 24. L. Dong, S.J. Wang, X.R. Zhao, Y.F. Zhu, J.K. Yu, 3D-printed poly(epsilon-caprolactone)  
418 scaffold integrated with cell-laden chitosan hydrogels for bone tissue engineering. *Sci. Rep.*  
419 7, 13412 (2017)
- 420 25. K.E. Michael, V.N. Vernekar, B.G. Keselowsky, J.C. Meredith, R.A. Latour, A.J. Garcia,  
421 Adsorption-induced conformational changes in fibronectin due to interactions with well-  
422 defined surface chemistries. *Langmuir* 19, 8033 (2003)
- 423 26. L. Corich, M. Buseti, V. Petix, S. Passamonti, A. Bandiera, Evaluation of a biomimetic  
424 3D substrate based on the Human Elastin-like Polypeptides (HELPS) model system for  
425 elastolytic activity detection. *J. Biotechnol.* 255, 57 (2017)
- 426 27. D.R. Yager, L.Y. Zhang, H.X. Liang, R.F. Diegelmann, I.K. Cohen, Wound fluids from  
427 human pressure ulcers contain elevated matrix metalloproteinase levels and activity  
428 compared to surgical wound fluids. *J. Invest. Dermatol.* 107, 743 (1996)
- 429 28. F. Grinnell, M. Zhu, Identification of neutrophil elastase as the proteinase in burn wound  
430 fluid responsible for degradation of fibronectin. *J. Invest. Dermatol.* 103, 155 (1994)
- 431 29. N.J. Trengove, M.C. Stacey, S. MacAuley, N. Bennett, J. Gibson, F. Burslem, G. Murphy,  
432 G. Schultz, Analysis of the acute and chronic wound environments: the role of proteases  
433 and their inhibitors. *Wound Repair Regen.* 7, 442 (1999)
- 434 30. C.J. Park, S.G. Clark, C.A. Lichtensteiger, R.D. Jamison, A.J. Johnson, Accelerated  
435 wound closure of pressure ulcers in aged mice by chitosan scaffolds with and without bFGF.  
436 *Acta Biomater.* 5, 1926 (2009)

437

# Tables and figures

**Table I.** Comparison of physical properties between CHIT/HEGF and CHIT.

	Swelling ratio (%)	Equilibrium water content (%)	Porosity (%)	Apparent density (mg/cm <sup>3</sup> )
CHIT	494.4±72.2	82.6±1.3	–	–
CHIT/HEGF	1125.0±52.9	90.7±1.5	36.77±5.97	41.83±3.34

**Figure 1.** (a) Schematic representation (not in scale) of the 3D-printed structure, (b) macroscopic appearance of a 3D-printed CHIT scaffold after ionotropic gelation in KOH 1.5 M, (c) lyophilized CHIT 3D-printed scaffold, and d) CHIT/HEGF composite after freeze-drying visualized by stereoscopic microscope.

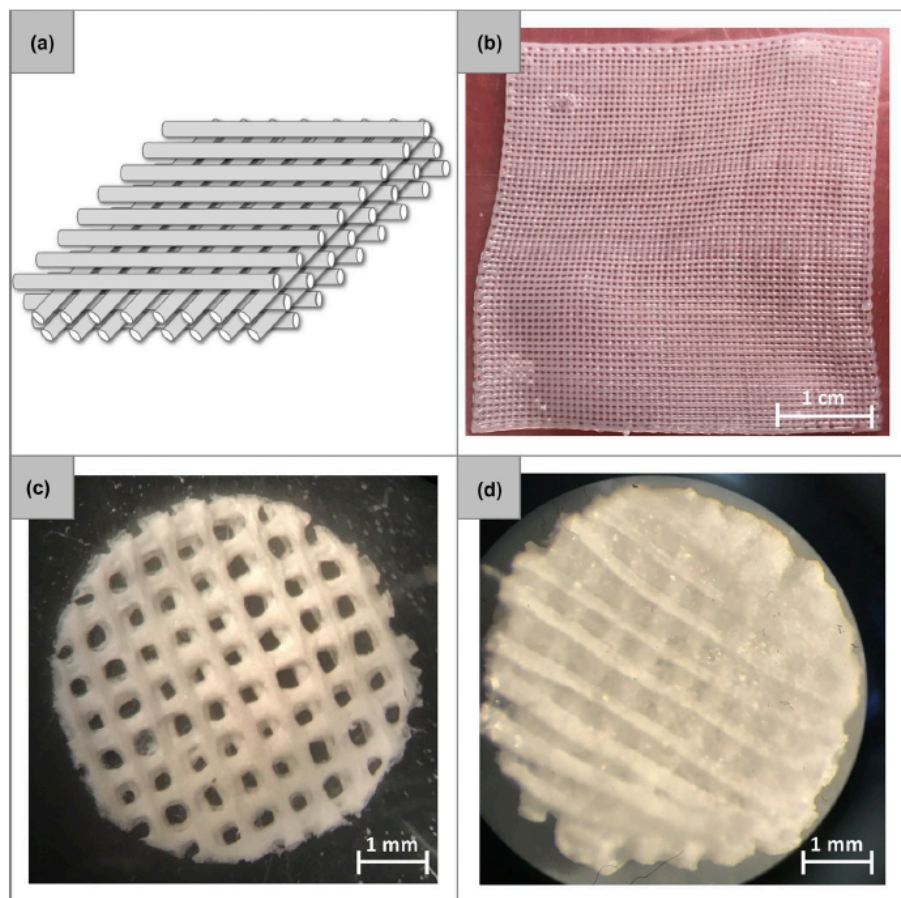




**Figure 2.** Representative SEM images of the CHIT/HEGF composite. The morphological differences are particularly evidenced in the magnification, where the HEGF-loaded HELP matrix form an open cell structure with an average diameter of  $86.5 \pm 23.3 \mu\text{m}$ , while the CHIT scaffold has a smaller interconnected network characterized by pores with elongated shape and an average diameter of  $30.3 \pm 10.9 \mu\text{m}$ .

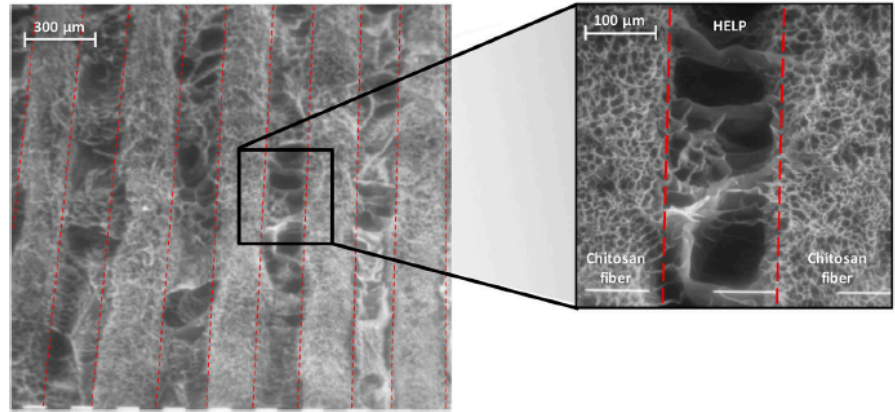


**Figure 3.** Physico-chemical and biological characterization of the 3D-printed chitosan scaffold (CHIT) and of CHIT/HEGF composite wound dressings. (a) Water uptake, (b) stability of the CHIT and CHIT/HEGF in SWF containing elastase, (c) cumulative release of EGF from CHIT/HEGF composites, (d) effect of the CHIT/HEGF on fibroblast viability. Bars represent the mean  $\pm$  SD of triplicate determination in three independent experiments.

